Journal of Nuclear Materials 407 (2010) 55–58

Contents lists available at ScienceDirect

Journal of Nuclear Materials

journal homepage: www.elsevier.com/locate/jnucmat

Evolution of fission-gas-bubble-size distribution in recrystallized U–10Mo nuclear fuel ☆

J. Rest

Argonne National Laboratory, 9700 S. Cass Ave., Argonne, IL 60439-4841, USA

A B S T R A C T

An analytical model for the nucleation and growth of intra and intergranular fission-gas bubbles, used to characterize fission-gas bubble development in U–Mo alloy fuel with burnup limited to less than 10 at.% U in order to capture the fuel swelling stage prior to irradiation-induced recrystallization, is extended to recrystallized fuel at a burnup of ~16 at.% U. During recrystallization the grain size is transformed from micron to sub-micron sizes. The intergranular bubble-size distribution post-recrystallization is found to evolve with similar kinetics and morphology to that pre-recrystallization with any differences primarily due to gas content and initial and/or boundary conditions (e.g., fuel microstructure). The predictions of the theory are compared with measured bubble-size distributions in pre and post recrystallized U–10Mo alloy fuel.

1. Introduction

In a recent paper [1], an analytical model for the nucleation and growth of intra and intergranular fission-gas bubbles was used to characterize fission-gas bubble development in low-enriched U–Mo alloy fuel irradiated in the advanced test reactor in Idaho as part of the Reduced Enrichment for Research and Test Reactor (RERTR) program. Fuel burnup was limited to less than 10 at.% U in order to capture the fuel swelling stage prior to irradiation-induced recrystallization. Calculations of intergranular bubble-size distributions for the range of burnup from 5.8 to 9.2 at.% U, fission rate from 2.3 to 6.8 $\times$ 10^{14} f/cm^3 s, temperature from 66 to 191 °C, and Mo content from 6 to 10 wt.% made with this mechanistic model of grain-boundary bubble formation kinetics are consistent with the measured distributions.

The model couples the calculation of the time evolution of the average intergranular bubble radius and number density to the calculation of the intergranular bubble-size distribution based on differential growth rate and sputtering coalescence processes. Analytical solutions were obtained to the rate equations thus providing for increased transparency and ease of use. The results support a multi-atom gas-bubble nucleation mechanism on grain boundaries that have substantially higher gas solubility than that in the grain interior. The gas-atom diffusion enhancement factor on the grain boundaries was estimated based on reasonable agreement with the measured distributions. The enhancement factor is about eight times higher for as-fabricated powder plates than for annealed plates due to the lower Mo content on the boundaries. The estimated range of values for the enhancement factor is consistent with values obtained in the literature [2].

The agreement between the model and the measured intergranular bubble-size distributions supports the validity of a sputtering coalescence (bubble coalescence without bubble motion) coarsening mechanism on the grain boundaries. In this regard, attempts by this author to reproduce the shape of the intergranular bubble-size distribution using a model based on the growth of bubbles in a regular array [3] have not been successful.

Previously, a number of the critical parameters used in the model were assumed to be the same as those listed in the literature for UO_2. However, it is the ratio of these parameters that appear in the model solution [1]; thus, the validity of their use for U–Mo reduces to the ratios being approximately the same for both materials. This assumption is supported by the observed similarity (albeit remarkable) in bubble behavior and microstructure evolution between the two materials [4].

The results demonstrate the increased validation leverage secured with the use of bubble-size distributions compared with the use of mean values (i.e. average quantities such as bubble density and diameter). Model predictions are sensitive to various materials and model parameters. Improved prediction capability requires an accurate quantification of these critical materials properties and measurement data.

This paper explores the bubble behavior in fuel that is pushed in burnup past the point where irradiation-induced recrystallization occurs. In contrast to the formation and subsequent growth of a recrystallized rim region in UO_2, irradiation-induced

☆ Work supported by US Department of Energy, Office of Global Threat Reduction, National Nuclear Security Administration (NNSA), under Contract DE-AC-02-06CH11357.

E-mail address: jrest@anl.gov

0022-3115/$ - see front matter © 2010 Elsevier B.V. All rights reserved.
doi:10.1016/j.jnucmat.2010.07.009

recrystallization occurs throughout U–Mo fuel due to the absence of a strong burnup gradient (the fuel is irradiated in relatively thin plates). During recrystallization the grain size is transformed from micron to sub-micron sizes. In general, the calculation of the intergranular gas-bubble distribution is independent of grain size. Thus, the bubble distribution subsequent to recrystallization should evolve with the same physical kinetics as dominates the bubble evolution prior to recrystallization. Given this, one would expect measured distributions post-recrystallization to be approximately similar to those pre-recrystallization with any differences being due to gas content and initial and/or boundary conditions. The predictions of the theory are compared with measured bubble distributions in pre and post recrystallized U–Mo alloy fuel.

2. Onset of recrystallization in U–10Mo fuel

Recrystallization nuclei are taken as the triple points of an evolving cellular dislocation network. The relevant dislocation kinetics comprises those of interstitial-loop formation and agglomeration that lead to the formation of a dislocation network in an environment of precipitate pinning [5]. The trigger point for irradiation-induced recrystallization is defined as the point where the kinetically derived concentration of nuclei becomes equal to the equilibrium number of nuclei determined from thermodynamic considerations.

The critical fission density F_{dx} at which recrystallization will occur is given by

$$F_{dx} = \left(\frac{\alpha_p \rho_d(T)}{\varphi\gamma}\right)^{4/5} \left(\frac{2\lambda}{3 b_v D_0 \beta}\right)^{1/5} \times \frac{f(v)^{6/5} \exp\left[4(\varepsilon_v/2 - \varepsilon_i)/15kT\right]}{\pi^{9/5}(C_A C_\rho)^{12/5}}, \quad (1)$$

where $\rho_d(T)$ is the temperature-dependent dislocation density, $\varphi\gamma/\alpha_p$ is a factor composed of terms related to the production of precipitates and sub-grain growth in the presence of precipitates, b_v is the van der Waals constant, λ is the atom knock-on distance, $f(v) = (1 - v/2)/(1 - v)$, v is Poisson's ratio, C_A is 3 for cubic cells, C_ρ is within a factor of unity, β is the number of gas atoms produced per fission, ε_i and ε_v are the interstitial and vacancy migration enthalpies, respectively, and where, at the relatively low temperatures T where irradiation-induced recrystallization occurs, the gas-atom diffusivity is athermal and can be expressed as $D_g = D_0\dot{f}$, where D_0 is a constant of proportionality and $\dot{f}$ is the fission rate. The fission density at which recrystallization is predicted to initiate as given by Eq. (1) is athermal and very weakly dependent on fission rate. As such, F_{dx} is independent of ε_v and ε_i and depends primarily on the collision related parameters λ, D_g and $\alpha_p/\varphi\gamma$. Substituting nominal values of the parameters corresponding to U–10Mo in Eq. (1) leads to the simplified expression for F_{dx} (m^{-3}):

$$F_{dx} \approx 6 \times 10^{24} (\dot{f})^{2/15}. \quad (2)$$

3. Grain size of recrystallized U–10Mo fuel

The calculation of recrystallized grain size [5] depends on the ratio of the materials surface energy γ to the elastic modulus E, the network dislocation density ρ_N, and the change in configurational entropy ΔS, i.e.

$$d_g^x = \frac{(12)^3 \gamma f(v)}{\sqrt{2}\pi b_v E (C_A C_\rho)^2 \rho_N^{1/2} + 2\sqrt{2}(12)^2 b_v^{-1} f(v) T \Delta S \rho_N^{-1/2}}, \quad (3)$$

where the network dislocation density is given by

$$\rho_N(t) = \frac{c_1}{c_2}\left[\frac{1 - e^{\sqrt{c_1 c_2}t}}{1 + e^{\sqrt{c_1 c_2}t}}\right]^2, \quad (4)$$

where

$$c_1 = \left[\pi v_l \frac{\sqrt{2}}{2} D_i c_i^2 / \Omega^{5/3}\right]^{1/2}, \quad (5)$$

and

$$c_2 = \frac{v_l (f(v)/\pi)^{1/2}}{C_A C_\rho}, \quad (6)$$

where v_l is the interstitial-loop climb controlled glide velocity, i.e.

$$v_l = \frac{2Z_{iv}}{b_v} D_i c_i. \quad (7)$$

The steady-state concentration of interstitials is given by

$$c_i = \frac{1}{D_i}\left(\frac{\Omega D_v K}{4\pi r_{iv}}\right)^{1/2}, \quad (8)$$

where K is the damage rate in atomic displacements per atom ($K \approx \dot{f}/10^{23}$), D_i and D_v the interstitial and vacancy diffusivity, respectively, Z_{iv} is the relative bias between interstitials and vacancies, and r_{iv} the defect recombination distance. The time t in Eq. (4) at the point where recrystallization occurs can be obtained from Eq. (2).

4. Calculation of bubble-size distributions in pre and post recrystallized U–10Mo fuel

Due to the strong effect of irradiation-induced gas-atom re-solution, in the absence of geometric contact, the intragranular bubbles stay in the nanometer size range. The density of bubbles increases rapidly early in the irradiation. At longer times, the increase in bubble concentration occurs at a much-reduced rate. Based on the above considerations, a quasi steady-state solution for the average intragranular bubble density c_b and the average number of gas atoms per bubble m_b as a function of the density of gas in solution c_g and the gas-atom radius r_g is given by [1]

$$c_b = \frac{16\pi f_n r_g D_g c_g^2}{b m_b(t)}, \quad (9)$$

$$m_b(t) = \left(\frac{3b_v}{4\pi}\right)^{1/2}\left(\frac{4\pi D_g c_g(t)}{b}\right)^{3/2}. \quad (10)$$

In Eq. (9), f_n is the bubble nucleation factor corresponding to a 2 atom nucleation mechanism, and b is the gas-atom re-solution rate. In general, the value of f_n is less than one reflecting the premise that gas-bubble nucleation within the fuel matrix requires the presence of vacancies/vacancy clusters in order to become viable. The average bubble radius r_b is related to m_b through the gas law and the capillarity relation. Imposing gas-atom conservation, i.e. requiring that the sum of the gas in solution, in intragranular bubbles, and on the grain boundary is equal to the amount of gas generated (there is no gas released from the U–Mo fuel), the term $c_g(t)$ is determined as

$$c_g(t) = \frac{-1 + \left[1 + 64\pi(1 - f_s) f_n r_g D_g \dot{f}\beta t/b\right]^{1/2}}{32\pi f_n r_g D_g/b}, \quad (11)$$

where β is the number of gas atoms produced per fission event and f_s is the fraction of gas released to the grain boundaries of grains of diameter d_g, where, following Speight [6]

$$f_s \approx \frac{8}{d_g}\left(D_g \frac{b}{b+g} t\right)^{1/2} - \frac{6}{d_g^2} D_g \frac{b}{b+g} t, \quad (12)$$

where $g = 4\pi D_g r_b c_b$.

In general, the solubility of gas on the grain boundary is substantially higher than in the bulk material. The gas concentration

on the boundary will increase until the solubility limit is reached whereupon the gas will precipitate into bubbles. Subsequent to bubble nucleation, gas solubility on the boundary will drop to a relatively low value and gas arriving at the boundary will be adsorbed by the existing bubble population [1]. The calculated intergranular bubble-size distributions are obtained by integrating the bubble-size-distribution function $n(r)$ over the bin sizes Δ_i, i.e. the bubble density $N(\Delta_i)$ in units of m^{-3} is

$$N(\Delta_i) = \int_{\Delta_0+(i-1)\Delta}^{\Delta_0+i\Delta} n(r)dr, \tag{13}$$

where,

$$n(r) = \frac{64\eta\gamma C_b^2\pi^2 r^3(kTr^3 + 3\gamma b_v r^2)\exp[-\kappa(r^4 - r_0^4)]}{3b_v C_g d_g(rkT + 2\gamma b_v)^2}, \tag{14}$$

and where

$$\kappa = \frac{\pi\dot{f}\lambda\delta}{2b_v\xi D_g C_g}. \tag{15}$$

In Eqs. (14) and (15), C_g and C_b are the mean gas-atom and gas-bubble concentration on the grain boundaries, respectively.

Following the work of Wood and Kear [7], grain-boundary bubble nuclei of radius R_b are produced until such time that a gas atom is more likely to be captured by an existing nucleus than to meet another gas atom and form a new nucleus. An approximate result for the mean grain-boundary bubble concentration is given by

$$C_b = \left(\frac{8zaK}{12^{1/3}\pi^2\xi D_g\delta}\right)^{1/2}. \tag{16}$$

In Eq. (16), a is the lattice constant, z is the number of sites explored per gas-atom jump, δ is the width of the boundary, ξ is a grain-boundary diffusion enhancement factor, and K is the flux of gas atoms per unit area of grain boundary,

$$K = \dot{f}\beta\frac{d_g}{3}\frac{d(f_s t)}{dt}, \tag{17}$$

Finally, the mean gas-atom concentration on the grain boundaries C_g is given by

$$C_g = \frac{d_g}{3}f_s\beta\dot{f}t. \tag{18}$$

5. Interpretation

In Table 1a description is listed of fuel used in the analysis: also listed are calculated values for F_{dx} given in Eq. (2), and d_g^x given in Eq. (3). V03 and V07 were irradiated to 5.8% and 7.4% U-atom burnup, respectively, and did not undergo irradiation-induced recrystallization. Plate 623 AD achieved ~15.6% U-atom burnup and was totally recrystallized. The calculated fission density F_{dx} at which recrystallization occurs is consistent with the observations. In addition, the calculated value for the size of the recrystallized grains d_g^x is within the range of measured values [5].

The values of the key parameters used in the model are given in Table 2. Many of them are known or estimated from the literature; the values of the others (e.g. ξ) result from comparison of the present theory with measured data for bubble populations. As an example of estimated parameters, the values of D_g and b used for U–Mo are assumed to be an order of magnitude less than those for UO_2. Based on irradiation-enhanced creep rates measured in UO_2, UN and UC [8], the irradiation-enhanced gas-atom diffusivity D_g is expected to be lower in U–Mo than in UO_2. In addition, due to the higher thermal conductivity of the alloy as compared to the oxide, b is also expected to be lower in U–Mo than in UO_2. This argument is based on the expected larger interaction cross section in the metallic alloy with conduction electrons. However, because of the (assumed) linear dependence of both D_g and b on $\dot{f}$, and because it is the ratio D_g/b that appears in Eqs. (9)–(11), it is reasonable to assume that this ratio of critical properties is approximately the same for both materials.

Table 2
Values of parameters used in the calculations.

Parameter	Value	Reference
β	0.25	Olander [10]
ξ	850	(non-annealed) this work
b_0 ($b = b_0\dot{f}$)	UO_2: 2×10^{-23} m^3	Spino/rest [11]
	U–10Mo: 2×10^{-24} m^3	This work
D_0 ($D_g = D_0\dot{f}$)	UO_2: 10^{-39} m^3 s^{-1}	Matzke [12]
	U–10Mo: 10^{-40} m^3 s^{-1}	This work
r_g	0.216 nm	Olander [10]
γ	0.5 J m^{-2}	(non-annealed) this work
$\cos(\theta)$	0.2	Hondros [2]
b_v	8.5×10^{-23} m^3/atom	Olander [10]
f_n	1	This work
δ_s	1×10^{-9} m	[1]
λ	1.8×10^{-8} m	[1]
Δ_0	2.5745×10^{-8} m	[1]
Δ_i	1×10^{-9} m	[1]

It should be noted that highly over pressurized solid gas bubbles with diameters of 1–2 nm were observed to form a superlattice in the U–Mo with a relatively close spacing (6–7 nm) and having an approximate mono-modal like distribution [9]. For this reason, as listed in Table 2, the gas-bubble nucleation factor was taken to be equal to unity. This assumption is augmented in light of the inability of the present formulation to capture the superlattice nature of the intragranular gas bubbles.

Fig. 1 shows the measured intergranular bubble-size distribution for U–10Mo as-atomized plates V07 and V03 [1]. The calculated distributions are in very good agreement with the measured quantities.

Fig. 2 shows the measured intergranular bubble-size distributions for U–10Mo as-atomized plate 623AD. The lines connecting data points for V07 and V03 from Fig. 1 are included for comparison. As evident from Fig. 2, for larger values of the fuel burnup, the bubble-size distribution broadens with the peak occurring at larger values of bubble concentration and bubble radius.

Also shown in Fig. 2 are the results of calculated bubble-size distribution using Eqs. (13)–(18) for plate 623AD. In order to account for the changing grain size during recrystallization, the calculation was approximated by the superposition of two solutions: (1) the bubble-size distribution was calculated using the as-fabricated grain size for the target burnup; and, (2) the bubble-size distribution was calculated over the burnup range from F_{dx} to F using the recrystallized grain size. This approximation

Table 1
Description of fuel used in the analysis: also listed are calculated values for F_{dx} and d_g^x.

Plate ID	Burn up (at.% U)	Fission rate (10^{20} f/m^3 s)	Fuel temp. (°C)	Fission density F (10^{27} f/m^3)	F_{dx}: Eq. (2) (10^{27} f/m^3)	Recrystallized/d_g^x: Eq. (3)
V07	5.8	4.8	122	2.0	3.4	No/–
V03	7.4	6.0	149	2.5	3.5	No/–
623AD	15.6	2.5	135	5.0	3.1	Yes/0.2 m

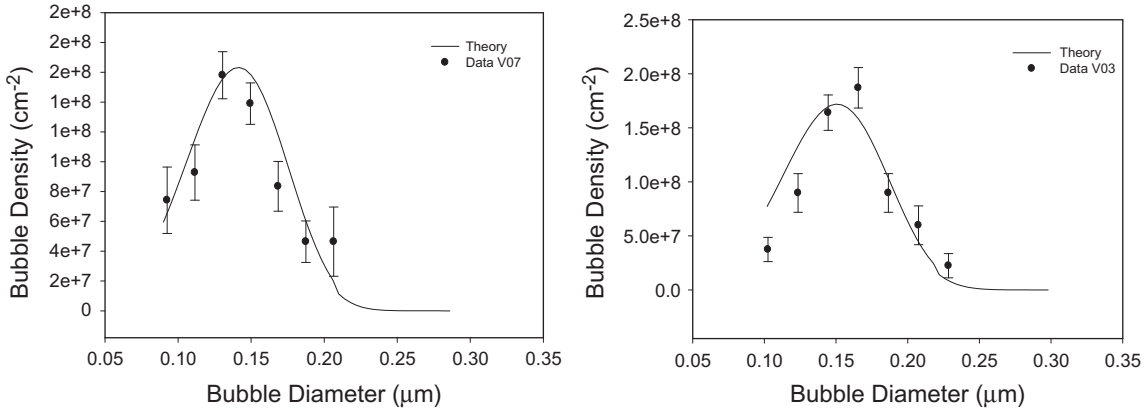

Fig. 1. Calculated and measured intergranular bubble-size distribution for plates V07 and V03.

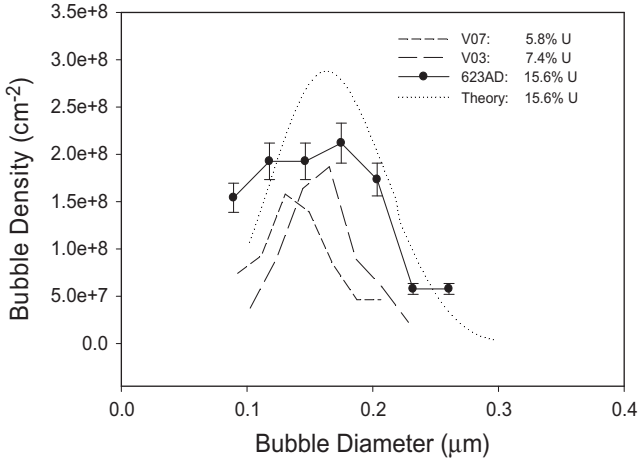

Fig. 2. Calculated and measured intergranular bubble-size distribution for plate 623AD. The lines connecting data points for V07 and V03 from Fig. 1 are included for comparison.

incorporates the assumption that the bubbles that grow on the original grain boundaries prior to irradiation-induced recrystallization are, for the most part, unaffected by the recrystallization process and subsequent fuel burnup. After the recrystallization event, bubbles form on the recrystallized grain boundaries in the same way as they previously formed on the original, larger grain boundaries. In general, the calculation of the intergranular gas-bubble-size distribution is independent of grain size. As is evident from Fig. 2, the calculated distributions follow the trend of the measurements.

6. Conclusions

Calculation of intergranular bubble-size distributions in U–10Mo alloy fuel made with a mechanistic model of grain-boundary bubble formation kinetics is consistent with the measured distributions pre and post irradiation-induced recrystallization. Analytical solutions are obtained to the rate equations thus providing for increased transparency and ease of use. The bubble distribution subsequent to recrystallization evolves with the same physical kinetics as dominates the bubble evolution prior to recrystallization. The results support the general feature that any differences in bubble evolution kinetics and morphology between pre and post irradiation-induced recrystallization regimes are due primarily to gas content and initial and/or boundary conditions (e.g., fuel microstructure).

Acknowledgements

The author would like to thank G.L. Hofman and Y. Soo Kim for assistance with the high-burnup bubble-distribution data.

References

[1] J. Rest, G.L. Hofman, Y. Soo Kim, J. Nucl. Mater. 385 (2009) 563.
[2] E.D. Hondros, in: K.C. Russell, H.I. Aaronson (Eds.), Precipitation Processes in Solids, The Metallurgical Society of AIME, 1976, p. 1.
[3] R.J. White, J. Nucl. Mater. 325 (2004) 61.
[4] G.L. Hofman, Y.S. Kim, Nucl. Eng. Technol. 37 (2005) 299.
[5] J. Rest, J. Nucl. Mater. 349 (2006) 150.
[6] M.V. Speight, Nucl. Sci. Eng. 37 (1969) 180.
[7] M.H. Wood, K.L. Kear, J. Nucl. Mater. 118 (1983) 320.
[8] G.L. Hofman, Y.S. Kim, A.B. Robinson, Fission Induced Swelling and Creep of Uranium–Molybdenum Alloy Fuel, in: Trans. 13th International Topical Meeting on Research Reactor Fuel Management, Vienna, 2009. ISBN: 978-92-95064-07-2.
[9] S. Van den Berghe, W. Van Renterghem, A. Leenaers, J. Nucl. Mater. 375 (2008) 340.
[10] D.R. Olander, Fundamental Aspects of Nuclear Reactor Fuel Elements, Technical Information Center, ERDA, USA, 1976.
[11] J. Spino, J. Rest, W. Goll, C.T. Walker, J. Nucl. Mater. 346 (2005) 131.
[12] Hj. Matzke, Radiat. Eff. 53 (1980) 219.